Weak boundary anchoring, twisted nematic effect, and homeotropic to twisted-planar transition

Wei Zhao, Chen-Xu Wu, and Mitsumasa Iwamoto*
Department of Physical Electronics, Tokyo Institute of Technology, 2-12-1 O-okayama, Meguro-ku, Tokyo 152-8552, Japan
(Received 27 February 2001; revised manuscript received 8 November 2001; published 13 February 2002)

Expansion analysis shows that in second order, the weak boundary coupling of nematic liquid crystals should be depicted by two anchoring coefficients and an orthonormal vector triplet. Using this binomial anchoring energy, we have derived the analytical expression of the threshold and saturation properties of the twisted nematic effect and the homeotropic to twisted-planar transition. Our results prove clearly that these two quite different transitions are reverse effects of each other.

DOI: 10.1103/PhysRevE.65.031709 PACS number(s): 61.30.Cz, 61.30.Gd

I. INTRODUCTION

Surface anchoring plays an essential role in the science and technology of liquid crystals. In the past several decades, many surface treatment techniques have been invented to build appropriate anchoring properties, such as rubbing, deposition of surfactants, oblique evaporation of SiO, etc. [1,2], and many methods have been developed to measure the anchoring energy relating to the liquid crystal-solid interface. Researchers have also made noteworthy attempts to construct proper mathematical descriptions of anchoring phenomena. So far many good results have been obtained [3]. However, the situation is not yet satisfactory. Many contradictory expressions of anchoring energy are in use today.

The analysis of field-induced structural transitions, such as the twisted nematic (TN) effect, is a significant subject in liquid crystal science. In general, structural transitions are attributed to the competition among the elastic energy of liquid crystal, the interaction of liquid crystal with the applied electric or magnetic field, and the surface anchoring energy. A proper expression of the anchoring energy is of critical importance for precise understanding of the structural transitions.

A monostable anchoring surface is schematically represented in Fig. 1. The easy axis $\vec{\epsilon}$ is in the (θ_e, ϕ_e) direction. As the surface director $\vec{n}_0$ deviates from $\vec{\epsilon}$, the surface energy g_s increases. As a function of spatial directions, the form of $g_s(\theta_0, \phi_0)$ is dependent on the nature of specific substrates. In practical investigation, many simple expressions have been employed in analyses of structural transitions of liquid crystals and anchoring transitions of substrate surfaces. Rapini and Papoular (RP) [4] originally introduced the trigonometric expression of the anchoring energy [Fig. 2(a)],

$$g_s = W \sin^2 \theta_0 . \tag{1}$$

This expression achieved much success in describing the homeotropic surface. However, a problem happens as it is applied to the planar and tilted anchoring surface, since the polar and azimuthal anchoring cannot be distinguished. Many types of generalizations of Eq. (1) have been made to describe the planar and tilted anchoring [5–10]. A simple and commonly used modification is to introduce directly a ϕ_0-dependent term. For tilted anchoring, it is assumed that

$$g_s = W_1 \sin^2(\theta_0 - \theta_e) + W_2 \sin^2(\phi_0 - \phi_e), \tag{2}$$

where the coefficients $W_{1,2}$ are the polar and azimuthal anchoring strengths, respectively. The problem with this expression is that it has two energy-minimized directions, (θ_e, ϕ_e) and $(\theta_e, \phi_e + \pi)$. This problem disappears for homogeneous planar anchoring and homeotropic anchoring. In these two cases, Eq. (2) is simplified to

$$g_s = W_1 \cos^2 \theta_0 + W_2 \sin^2 \phi_0 \tag{3}$$

and

$$g_s = W_1 \sin^2 \theta_0 + W_2 \sin^2 \phi_0 , \tag{4}$$

respectively. The polar diagrams of these three expressions are shown in Figs. 2(b)–2(d). The common feature of these expressions is the singularity along the normal $\hat{z}$ to the substrate as seen in the figures. In other words, the anchoring energy is not properly defined in the surface normal. In its origin, this is due to the unphysical dependence of Eqs. (2)–(4) on ϕ_0: The singularity is a result of the artificial separation of the anchoring energy into a θ_0-dependent part and a ϕ_0-dependent part [11].

A meaningful improvement was made by Beica *et al.* [10]. They proposed an expression of surface energy consisting of two square terms of inner products,

$$g_s = W_1'(\vec{n}_0 \cdot \vec{n}_1)^2 + W_2'(\vec{n}_0 \cdot \vec{n}_2)^2, \tag{5}$$

where $\vec{n}_1 = (\vec{\epsilon} \times \vec{z})/|\vec{\epsilon} \times \vec{z}|$ and $\vec{n}_2 = \vec{\epsilon} \times \vec{n}_1$. $(\vec{n}_1, \vec{n}_2, \vec{\epsilon})$ are the three principal axes of anchoring. Comparatively, this ex-

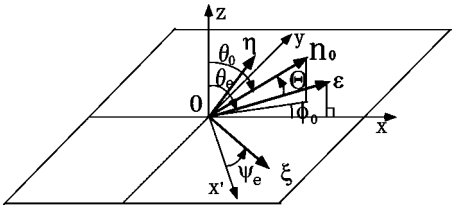

FIG. 1. Schematic of surface anchoring. In this figure, $\phi_e = 0$, and Φ (not labeled) is the angle between planes $\epsilon O\xi$ and $\epsilon O n_0$.

*Email address: iwamoto@pe.titech.ac.jp

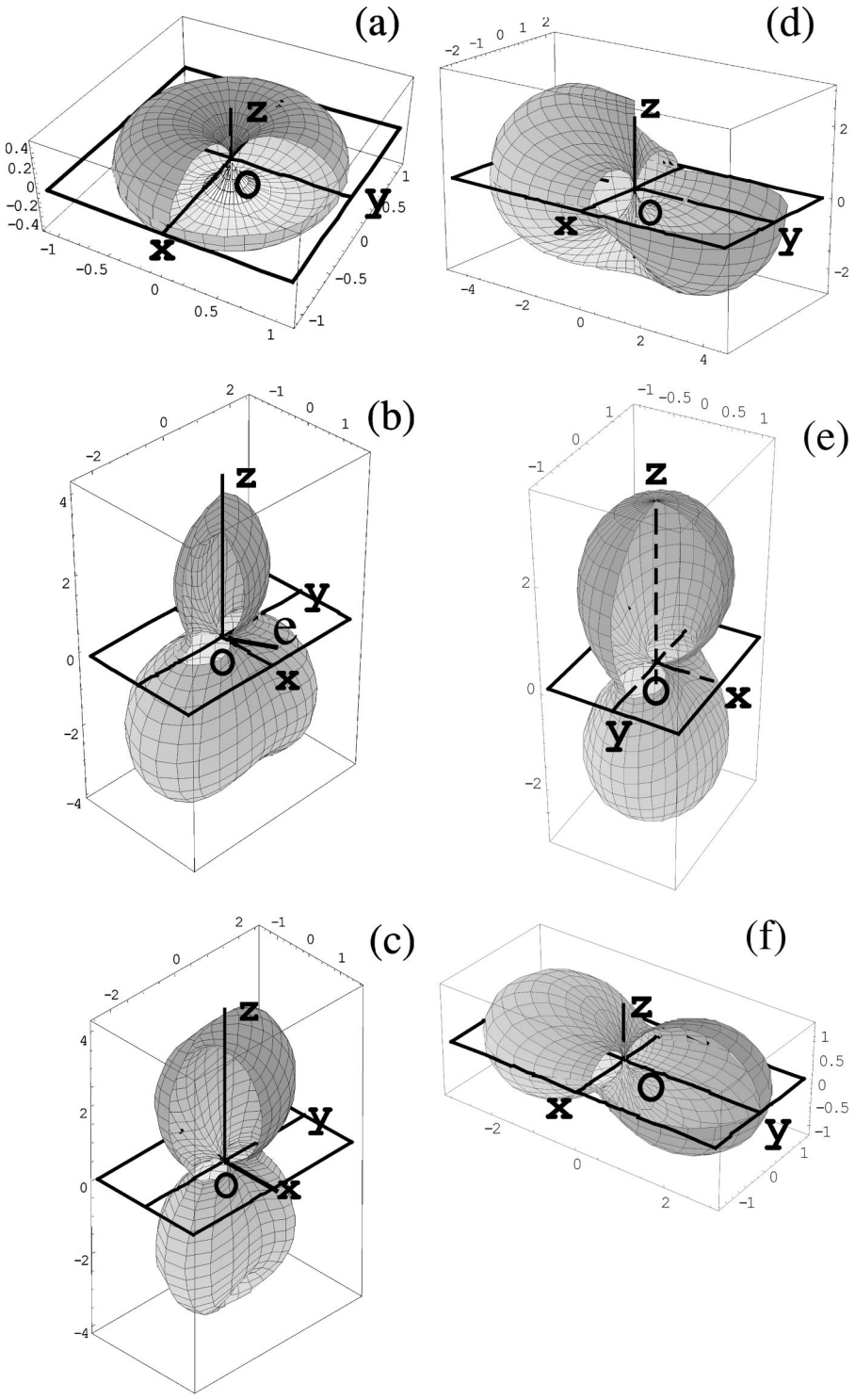

FIG. 2. Cut-away view of the polar diagrams of anchoring energy functions discussed in this paper. In each figure, the surface of the substrate is represented by the xOy plane; the length of the radius vector from the origin O to any point at the curved surface represents the interfacial energy g_s in that direction (in arbitrary units). (a) The RP expression Eq. (1), with $W=1$. This polar diagram is axisymmetric. (b) Equation (2) with $\theta_e=2\pi/5$, $\phi_e=0$, $W_1=3$, and $W_2=1$. This diagram is not centrosymmetric. There are two easy directions: One is denoted by ϵ, and the other is its mirror-symmetric vector with respect to the yOz plane. The singularity along the z axis is clear. (c) Equation (3) with $W_1=3$ and $W_2=1$; (d) Eq. (4) with $W_1=2$ and $W_2=2.5$. These two diagrams are centrosymmetric; yet, they are still singular along the z axis. (e) Equation (11) with $W_p=3$ and $W_a=1$; (f) Eq. (12) with $W_1=1$ and $W_2=3$. In these two centrosymmetric diagrams, the singularity existing in (b), (c), and (d) does not appear. These two diagrams, (e) and (f), are congruent, with the difference of only a rotation. For the common tilted anchoring expressed by Eq. (10), the corresponding polar diagram is the same as diagram (f) except for a Euler rotation (ϕ_e,θ_e,ψ_e).

pression is preferable to Eq. (2) since the problem of the presence of two degenerate easy directions is resolved. However, Eq. (5) is still incomplete, and in certain cases it gives wrong predictions. We give two examples. First, in the homeotropic anchoring case, $\vec{\epsilon}=\vec{z}$; according to their definitions, we get $\vec{n}_1=\vec{n}_2=0$. Consequently, Eq. (5) degenerates to $g_s=0$, and cannot depict the homeotropic surface. As a result, even RP's initial expression Eq. (1) is not included in Eq. (5). Second, recent finite-element simulation [12] found that the asymmetrically modulated surface, with in-plane easy axis along the grooving direction, may have principal axes of anchoring obliquely intersecting with the normal to the surface. This is in obvious contradiction with the argument of Beica *et al.,* since Eq. (5) predicts that if $\vec{\epsilon}=\vec{x}$, the anchoring triplet must be $(\vec{x},\vec{y},\vec{z})$.

In our recent work [13], we have proposed an expression of the anchoring energy through spherical harmonic expansion. Up to the second rank, an orthonormal vector triplet is naturally introduced, which consists of the three principal axes of anchoring. The subtle difference of this anchoring triplet from that introduced in Ref. [10] not only resolves the problems of Eq. (5), but also reveals more physical contents. Using this harmonic anchoring energy, we have also analyzed the TN effect and the voltage-controlled-twist effect [14], and obtained satisfactory results. In this paper, we show the versatility of this surface energy expression in more detail. The polar diagrams of the anchoring energy functions discussed in this article are shown in Fig. 2. We also give detailed derivation of the threshold and saturation properties of a twisted nematic liquid-crystal (TNLC) slab, and the homeotropic to twisted-planar (HTP) transition. The latter, invented recently, is of practical importance due to its superior optical properties in liquid-crystal displays. Our analyses show that these two structural transitions, though apparently very different, are intimately related in that their threshold and saturation properties are expressed by essentially identical but exchanged formulas, i.e., the formulas for the threshold property of the TN effect correspond to those of the saturation property of the HTP effect, and vice versa. This is convincing evidence for the conclusion that these two distinct transitions are actually reverse effects of each other.

II. EXPANSION OF SURFACE ENERGY

It should be emphasized that the equivalence of $\vec{n}$ and $-\vec{n}$ leads to centrosymmetry of the surface energy g_s,

$$g_s(\vec{n}_0)=g_s(-\vec{n}_0), \quad \text{or} \quad g_s(\theta_0,\phi_0)=g_s(\pi-\theta_0,\pi+\phi_0). \tag{6}$$

Consequently, g_s can be regarded as a function defined on the whole solid angle, though the liquid crystal exists only on one side of the interface. As a direct result of the centrosymmetry, any odd-order terms disappear spontaneously in a series expansion of g_s.

It is instructive to examine the expressions given in Sec. I from the viewpoint of symmetry. Indeed, Eq. (2) is not a proper expression of the anchoring energy because it is not centrosymmetric, as represented in Fig. 2(b).

Consider the expansion of interfacial energy g_s of a monostable anchoring surface. g_s has two minima in $\vec{\epsilon}$ and $-\vec{\epsilon}$ directions. As a function of surface orientation, the interfacial energy g_s has been expanded into spherical harmonics by Pieranski and Jérôme, in the analysis of an anchoring transition [15], where the surface normal $\hat{z}$ was employed naturally as the polar axis of the spherical coordinate. Different from Ref. [15], in this paper, the easy axis $\vec{\epsilon}$ will be employed as the polar axis of the spherical harmonics. Although this mathematical technique does not lead to essential difference, it does simplify the treatment and the form of the result. We have

$$g_s(\Theta,\Phi)=\sum_{l=0,2,4\cdots}\sum_{m=-l}^{l} g_{lm}Y_{lm}(\Theta,\Phi), \quad g_{l-m}=g_{lm}^*, \tag{7}$$

where Θ and Φ are the polar and azimuthal angles with respect to $\vec{\epsilon}$ (Fig. 1). The starting direction of the azimuthal angle Φ is to be determined later.

In Eq. (7), the $(lm=00)$ term is the isotropic part and can be discarded. Since $Y_{20}(\Theta,\Phi)=(3\cos^2\Theta-1)/2$, the $(lm=20)$ term contributes an energy term which corresponds to the single-constant energy highlighted by Sugimura *et al.* [9]

$$\cos^2\Theta=(\vec{n}_0\cdot\vec{\epsilon})^2. \tag{8}$$

Now consider the $(lm=2\pm1)$ couple. Writing $G_{21}\equiv g_{21}Y_{21}(\Theta,\Phi)+\text{c.c.}$, where $Y_{21}=\sin\Theta\cos\Theta e^{i\Phi}$, we have

$$\left[\frac{\partial G_{21}}{\partial\Theta}\right]_{\Theta=0}=g_{21}e^{i\Phi}+\text{c.c.}\neq 0.$$

This is in contradiction with the fact that the easy axis $\vec{\epsilon}$ $(\Theta=0)$ is a stationary direction. So we conclude that $g_{21}=0$. This significant simplification is indeed originated from the employment of $\vec{\epsilon}$ as the polar axis of the spherical harmonics. As for the $(lm=2\pm2)$ couple, we have

$$g_{22}Y_{22}(\Theta,\Phi)+\text{c.c.}=4|g_{22}|\sin^2\Theta\cos^2\Phi-2|g_{22}|\sin^2\Theta, \tag{9}$$

where, without loss of generality, the starting azimuthal direction $\Phi=0$ has been chosen especially to offset the argument of g_{22}. Merging the second term on the right-hand side of Eq. (9) with Eq. (8), and redefining the coefficients, we get the second-order anchoring energy

$$\begin{aligned} g_s(\Theta,\Phi)&=W_\xi\sin^2\Theta\cos^2\Phi+W_\eta\sin^2\Theta\sin^2\Phi \\ &=W_\xi(\vec{n}\cdot\vec{\xi})^2+W_\eta(\vec{n}\cdot\vec{\eta})^2, \end{aligned} \tag{10}$$

where the unit vectors $\vec{\xi}$ and $\vec{\eta}$, together with the easy axis $\vec{\epsilon}$, are the stationary directions of the second-order anchoring energy. The orthonormal vector triplet $(\vec{\xi},\vec{\eta},\vec{\epsilon})$ is of Euler

angles $(\phi_e, \theta_e, \psi_e)$ with respect to the elementary triplet $(\hat{x}, \hat{y}, \hat{z})$ (Fig. 1). W_ξ (W_η) is the energy difference between $\vec{\xi}$ $(\vec{\eta})$ and $\vec{\epsilon}$ directions.

Equation (10) offers a simple and clear description of the anisotropic interfacial energy. Formally it is analogous to Eq. (5). It is worthy to emphasize the difference between them: Equation (5) depicts only the special case with $\psi_e = 0$, yet our present expression applies to arbitrary monostable tilted anchoring cases, including the $\psi_e \neq 0$ case.

Now we discuss some special cases. Consider the homogeneous planar anchoring. Assuming $\vec{\epsilon} = \vec{x}$, we know that $\vec{\xi}$ and $\vec{\eta}$ are two unit vectors in the yOz plane. According to the symmetry of the surface, two cases should be discussed separately. (a) Anchoring surface without $y \leftrightarrow -y$ mirror symmetry. Therefore, in general $\psi_e \neq 0$, and $\vec{\xi}$ and $\vec{\eta}$ intersect obliquely with the $\hat{z}$ axis. This is just the planar anchoring case studied by Brown *et al.* through numerical simulation [12]. Their results revealed that a substrate surface treated by asymmetric grooving may have two stationary directions (not the easy axis) intersecting with the surface normal obliquely, whereas they are still perpendicular to each other and perpendicular to the easy axis (the grooving direction). These features are in good agreement with the predictions of our present analysis. (b) Anchoring surface with $y \leftrightarrow -y$ mirror symmetry. In this case, $\psi_e = 0$, Eq. (10) becomes

$$g_s = W_p(\vec{n}_0 \cdot \hat{z})^2 + W_a(\vec{n}_0 \cdot \hat{y})^2 = W_p \cos^2\theta_0 + W_a \sin^2\theta_0 \sin^2\phi_0, \tag{11}$$

where W_p and W_a are the polar and azimuthal anchoring strengths, respectively. The polar diagram of this expression is shown in Fig. 2(e). We find that the singularity along the surface normal seen in Fig. 2(c) does not appear in Fig. 2(e).

In the homeotropic anchoring case, $\vec{\epsilon} = \hat{z}$, Eq. (10) is simplified to [Fig. 2(f)]

$$g_s = W_1(\vec{n}_0 \cdot \hat{x})^2 + W_2(\vec{n}_0 \cdot \hat{y})^2 = W_1 \sin^2\theta_0 \cos^2\phi_0 + W_2 \sin^2\theta_0 \sin^2\phi_0. \tag{12}$$

If the surface is isotropic in the plane, $W_1 = W_2$, RP's initial expression is obtained. On the other hand, Refs. [8] and [14] offered examples of homeotropic substrate whose in-plane isotropy was broken by rubbing or photolithographic grooving. Their surface energy is expressed by Eq. (12) properly. Comparing to Fig. 2(d), the polar diagram of Eq. (12), as shown in Fig. 2(f), is not singular along the z axis.

In the tilted anchoring case, if $\psi_e = 0$, Eq. (10) returns to Eq. (5). In general, a nontrivial ψ_e means that none of the three stationary directions of the surface energy is located on the substrate surface. So far we have never noticed any reports of observations of this kind of effect. Asymmetrical grooving or oblique evaporation of SiO on a solid surface in intersected directions may realize it.

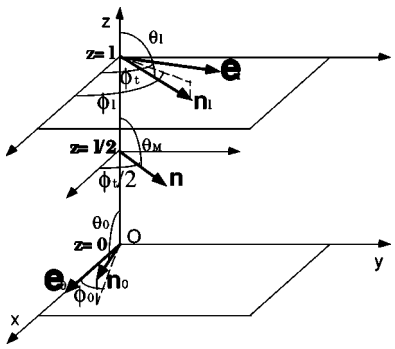

FIG. 3. Schematic of the twisted nematic slab fabricated between the two planes $z = 0$ and l.

III. FIELD-CONTROLLED TWISTED NEMATIC TRANSITION

A. Torque balance equations

In this section, we analyze the structural transition of a TNLC slab sandwiched between two identical substrates with homogeneous planar anchoring, located at $z = 0$ and l, respectively (Fig. 3). The upper substrate is rotated at angle ϕ_t with respect to the lower one. The anchoring energy of the lower and upper substrates are expressed as

$$g_s^0 = W_p \cos^2\theta_0 + W_a \sin^2\theta_0 \sin^2\phi_0, \qquad g_s^l = W_p \cos^2\theta_l + W_a \sin^2\theta_l \sin^2(\phi_l - \phi_t), \tag{13}$$

respectively, where $\theta_{0,l}$ and $\phi_{0,l}$ are the boundary values of the orientation angles θ and ϕ. An electric field is applied perpendicular to the plates. The Gibbs free energy of the liquid-crystal cell is the sum of the bulk energy and the surface energy. In the problem that we are concerned with, the director $\vec{n}$ is only dependent on z. In the continuum theory, the free energy per unit area of the TNLC slab is expressed as [16]

$$f = \int_0^l g_e dz - \frac{1}{2}\int_0^l \vec{D} \cdot \vec{E} dz + g_s^0 + g_s^l, \tag{14}$$

where the two boundary couplings are manifested as additive terms. This simplifies the variational calculation. The first integral in Eq. (14) is the elastic energy of nematic liquid crystals, with

$$g_e = \frac{1}{2}[k_{11}(\nabla \cdot \vec{n})^2 + k_{22}(\vec{n} \cdot \nabla \times \vec{n} + 2\pi/p_0)^2 + k_{33}[\vec{n} \times (\nabla \times \vec{n})]^2] = \frac{1}{2}[f(\theta)\theta^{(1)2} + h(\theta)\phi^{(1)2}] + k_2 \sin^2\theta\phi^{(1)} + \frac{k_2^2}{2k_{22}}, \tag{15}$$

where k_{11}, k_{22}, and k_{33} are the splay, twist, and bend elastic constants of the liquid crystal, respectively, p_0 denotes the

pitch of the material, $k_2=-2\pi k_{22}/p_0$ is the chiral elastic modulus, $\theta^{(1)}=d\theta/dz$, $\phi^{(1)}=d\phi/dz$, and

$$f(\theta)=k_{11}\sin^2\theta+k_{33}\cos^2\theta,$$
$$h(\theta)=\sin^2\theta(k_{22}\sin^2\theta+k_{33}\cos^2\theta). \tag{16}$$

The second integral in Eq. (14) is the dielectric energy

$$-\frac{1}{2}\int_0^l \vec{D}\cdot\vec{E}dz=-\frac{V^2}{2}\left[\int_0^l \frac{dz}{\epsilon_\perp+\epsilon_a\cos^2\theta}\right]^{-1}\equiv-\frac{V^2\overline{\epsilon}}{2l}, \tag{17}$$

where $\epsilon_a=\epsilon_\parallel-\epsilon_\perp$ is the dielectric anisotropy of the liquid-crystal material. The quantity $V\overline{\epsilon}/l=\sigma=D_z$ is indeed the surface density σ of the electric charge on the substrates, or the z component D_z of the dielectric displacement, which is constant across the liquid-crystal cell.

The torque balance equations can be constructed through minimization of the free-energy Eq. (14). A brief variational calculation $\delta f=0$ and subsequent integration generate two bulk equations and two boundary conditions for the lower-substrate surface

$$f(\theta)\theta^{(1)2}+\frac{(C_1-k_2\sin^2\theta)^2}{h(\theta)}-\frac{D_z^2}{\epsilon_\perp+\epsilon_a\cos^2\theta}=C_2, \tag{18}$$

$$\phi^{(1)}=(C_1-k_2\sin^2\theta)/h(\theta), \tag{19}$$

$$f(\theta_0)\theta^{(1)}|_{z=0}+(W_p-W_a\sin^2\phi_0)\sin 2\theta_0=0, \tag{20}$$

$$h(\theta_0)\phi^{(1)}|_{z=0}+k_2\sin^2\theta_0-W_a\sin^2\theta_0\sin 2\phi_0=0, \tag{21}$$

where C_1 and C_2 are constants of integration. For reasons of symmetry, the boundary conditions for the upper substrate are essentially the same as those for the lower one. Also owing to symmetry, we have, at the midplane

$$\theta^{(1)}|_{z=l/2}=0,$$
$$\theta(l/2)=\theta_M, \tag{22}$$
$$\phi(l/2)=\phi_t/2,$$

where θ_M is dependent on the applied voltage V.

Equations (18)–(22) are the basic relations for solving the director distribution and the threshold and saturation properties of the TNLC slab. Comparatively, the two bulk equations are the same as those derived previously, while the boundary conditions are more complicated than the corresponding equations obtained in Refs. [4–7,9,17], for in the present equations the two orientation angles θ_0 and ϕ_0, and the two anchoring coefficients, W_p and W_a, are all entangled together.

The integration of Eqs. (18)–(22) generates

$$C_1=W_a\sin^2\theta_0\sin 2\phi_0, \tag{23}$$

$$\frac{l}{2}=\int_{\theta_0}^{\theta_M}N^{1/2}(\theta)d\theta, \tag{24}$$

$$\frac{\phi_t}{2}-\phi_0=\int_{\theta_0}^{\theta_M}h^{-1}(\theta)(C_1-k_2\sin^2\theta)N^{1/2}(\theta)d\theta, \tag{25}$$

$$f(\theta_0)N^{-1/2}(\theta_0)=-(W_p-W_a\sin^2\phi_0)\sin 2\theta_0, \tag{26}$$

where $N(\theta)$ is defined by

$$N(\theta)=f(\theta)\left[\frac{\epsilon_a D_z^2(\cos^2\theta_M-\cos^2\theta)}{(\epsilon_\perp+\epsilon_a\cos^2\theta_M)(\epsilon_\perp+\epsilon_a\cos^2\theta)}+\frac{(C_1-k_2\sin^2\theta_M)^2}{h(\theta_M)}-\frac{(C_1-k_2\sin^2\theta)^2}{h(\theta)}\right]^{-1}. \tag{27}$$

For a given voltage V, the values of θ_0, ϕ_0, and θ_M can be determined by Eqs. (23)–(26).

B. Fréedericksz transition

The threshold and saturation properties of a TN cell can be obtained through observing the behavior of θ_M. At the threshold voltage V_F, θ_M begins to deviate from $\pi/2$; at the saturation voltage V_S, θ_M approaches 0 and the liquid-crystal director becomes homeotropic.

To derive the threshold property of the Fréedericksz transition, we suppose $\theta_0=\theta_M=\pi/2$ for $V<V_F$ and $\theta_M\to\pi/2$ when $V\to V_F$. In this extreme case, Eqs. (23)–(26) can be solved analytically. It is convenient to introduce the dimensionless parameters,

$$\lambda=\pi k_{11}/(2lW_p),$$
$$\gamma=W_a/W_p, \tag{28}$$
$$u_F=V_F/V_c,$$

where $V_c=\pi\sqrt{k_{11}/\epsilon_a}$ is the threshold voltage of an untwisted nematic slab ($\phi_t=0$) with rigid boundary coupling ($W_a\to\infty, W_p\to\infty$). After a lengthy derivation (see the Appendix for more details), we get three equations defining the threshold property of the TN effect,

$$\phi_t-2\phi_0^F-\frac{2\pi l}{p_0}=\frac{\pi\gamma k_{11}}{2\lambda k_{22}}\sin 2\phi_0^F, \tag{29}$$

$$1-\gamma\sin^2\phi_0^F=\lambda X\tan(\pi X/2), \tag{30}$$

$$u_F=\left[X^2+\frac{(k_{33}-2k_{22})\Delta\phi^2}{k_{11}\pi^2}+\frac{4lk_{22}\Delta\phi}{p_0k_{11}\pi}\right]^{1/2}, \tag{31}$$

where ϕ_0^F is the threshold value of ϕ_0, and $\Delta\phi=\phi_t-2\phi_0^F$ the total twist of the liquid crystal director at the threshold. X is a subsidiary variable. u_F can be solved as X and ϕ_0^F has been obtained from Eqs. (29) and (30). Incidentally, in Eq.

(29) ϕ_0^F is indeed dependent only on the azimuthal anchoring strength W_a. Thus W_a can be determined if the threshold angle ϕ_0^F is measured [18].

It is instructive to compare the present paper with previous studies. Becker *et al.* [6] studied a substrate with strong azimuthal and weak polar couplings. In Eqs. (29)–(31), taking the limit $\gamma\to\infty$, we get $\phi_0^F=0$, and

$$\lambda X \tan(\pi X/2)=1, \tag{32}$$

$$u_F=\left[X^2+\frac{(k_{33}-2k_{22})\phi_t^2}{k_{11}\pi^2}+\frac{4lk_{22}\phi_t}{p_0k_{11}\pi}\right]^{1/2}. \tag{33}$$

This recovers the result reported by Becker *et al.* [6]. When $p_0\to\infty$, Eqs. (32) and (33) reduce to the corresponding formula given by Yang [17],

$$\lambda\left[u_F^2-\frac{(k_{33}-2k_{22})\phi_t^2}{k_{11}\pi^2}\right]^{1/2}\tan\left\{\frac{\pi}{2}\left[u_F^2-\frac{(k_{33}-2k_{22})\phi_t^2}{k_{11}\pi^2}\right]^{1/2}\right\}=1. \tag{34}$$

If we further take the equal-elastic-constant approximation, the result by Nehring *et al.* [5] is found,

$$(\lambda/\pi)(\phi_t^2+\pi^2u_F^2)^{1/2}\tan[(\phi_t^2+\pi^2u_F^2)^{1/2}/2]=1. \tag{35}$$

Now consider a TN cell consisting of strong anchoring substrates and an achiral liquid-crystal material. In the limit $\lambda\to0$, Eq. (34) becomes

$$u_F=\left[1+\frac{(k_{33}-2k_{22})\phi_t^2}{k_{11}\pi^2}\right]^{1/2}. \tag{36}$$

So we have returned to the result given by Leslie [19] and Schadt and Helfrich [20].

On the other hand, under the condition $\gamma=1$, Eqs. (29) and (30) become, respectively,

$$\phi_t-2\phi_0^F-\frac{2\pi l}{p_0}=\frac{\pi k_{11}}{2\lambda k_{22}}\sin 2\phi_0^F, \tag{37}$$

$$\cos^2\phi_0^F=\lambda X\tan(\pi X/2). \tag{38}$$

Together with Eq. (31), they precisely recover the result obtained by Sugimura *et al.* under the assumption of equal polar and azimuthal anchoring coefficients [9].

Figure 4 shows the λ and γ dependencies of the threshold voltage u_F and the surface twist angle ϕ_0^F of a TN cell, with $\phi_t=90°$, and $l/p_0=0$. The material parameters used in calculation are $k_{33}/k_{11}=1.5$,$k_{22}/k_{11}=0.6$. Five groups of curves are drawn, with $\gamma=\infty$, 1, 0.1, 0.01, and 0, respectively. The first two values of γ is to recover the results reported in Refs. [6] and [9], respectively. The next two values of γ is to simulate the more realistic cases in which the azimuthal anchoring is one or two orders weaker than the polar coupling. $\gamma=0$ is an extreme case, corresponding to the degenerate planar anchoring. It is clear from Fig. 4(a) that the threshold voltage is mainly dependent on λ, and

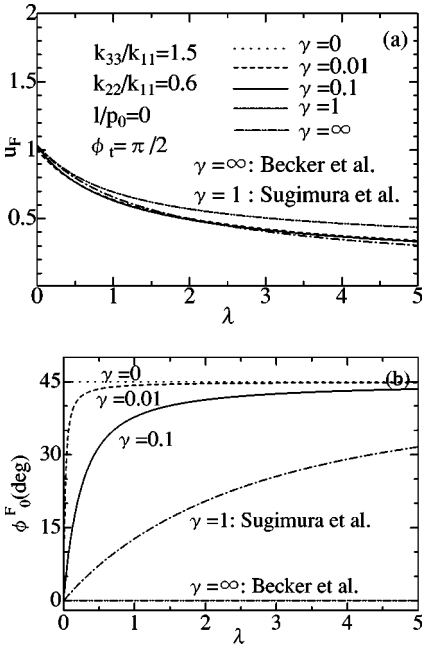

FIG. 4. λ and γ dependencies of the threshold property of a 90° twisted nematic slab. (a) The reduced threshold voltage u_F; (b) the surface twist angle ϕ_0^F at the threshold. As special cases, the results reported in Refs. [6] and [9] are plotted, with $\gamma=\infty$ and 1, respectively. The material parameters used are $k_{33}/k_{11}=1.5$, $k_{22}/k_{11}=0.6$, and $l/p_0=0$.

almost independent from γ. Comparatively, the γ dependency of the surface twist angle ϕ_0^F is far more remarkable. As shown in Fig. 4(b), with the decrease of γ from ∞ to 0, the $\phi_0^F-\lambda$ curve varies continuously from $\phi_0^F\equiv0$ to $\phi_0^F\equiv45°$. This implies that near the threshold the optical properties of the TNLC slab is strongly dependent on the azimuthal anchoring of the substrates.

C. Saturation properties

The saturation property of a TNLC slab can be analytically solved through treating Eqs. (23)–(26) in the limit $\theta_M\to0$ when $V\to V_S$. Through a lengthy calculation, we get three equations (see the Appendix for more details)

$$\sin^2 T=\frac{1}{\gamma}\cosh^2(\pi Y/2)\left[1-\frac{k_{33}\lambda Y}{k_{11}}\tanh(\pi Y/2)\right]\times\left[1-\frac{k_{11}(1-\gamma)}{k_{33}\lambda Y}\tanh(\pi Y/2)\right], \tag{39}$$

$$\tan\phi_0^S=\tan T\left[1-\frac{k_{11}}{k_{33}\lambda Y}\tanh(\pi Y/2)\right]\times\left[1-\frac{k_{11}(1-\gamma)}{k_{33}\lambda Y}\tanh(\pi Y/2)\right]^{-1}, \tag{40}$$

$$u_S=\left\{\frac{k_{33}}{k_{11}}\left[Y^2+\left(\frac{2lk_{22}}{p_0k_{33}}\right)^2\right]\right\}^{1/2}, \tag{41}$$

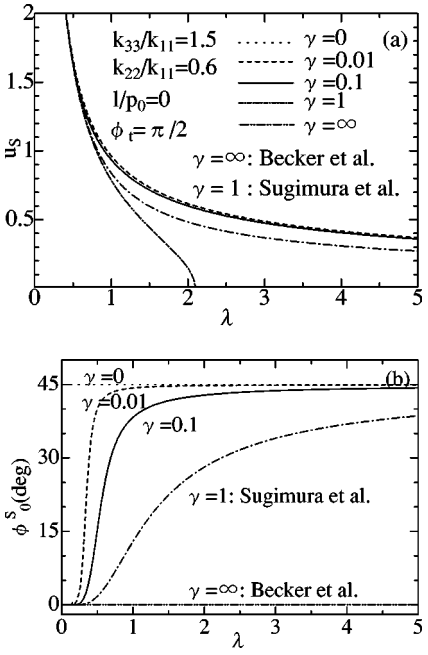

FIG. 5. λ and γ dependencies of the saturation property of a 90° twisted nematic slab. (a) The reduced saturation voltage u_S; (b) the surface twist angle ϕ_0^S at saturation. The curves with $\gamma=\infty$ and 1 recover the results reported in Refs. [6] and [9], respectively. The material parameters used are $k_{33}/k_{11}=1.5$, $k_{22}/k_{11}=0.6$, and $l/p_0=0$.

where $T=\phi_t/2-\pi l k_{22}/(p_0 k_{33})$, Y is a subsidiary variable, $u_S=V_S/V_c$ the reduced saturation voltage, and ϕ_0^S the surface twist angle at the saturation. Once Y has been found from Eq. (39), the saturation voltage u_S and the surface twist angle ϕ_0^S can be calculated using Eqs. (40) and (41).

To understand this complex result, we compare it with previous studies. In the limit $\gamma\to\infty$, Eq. (40) simply gives $\phi_0^S=0$, and Eq. (39) is reduced to

$$\sin^2 T=\frac{k_{11}}{k_{33}\lambda Y}\sinh(\pi Y/2)\cosh(\pi Y/2)\times\left[1-\frac{k_{33}\lambda Y}{k_{11}}\tanh(\pi Y/2)\right]. \tag{42}$$

This equation, together with Eq. (41), is consistent with the result reported in Ref. [6]. For equal-elastic-constant approximation and $p_0\to\infty$, Eqs. (41) and (42) are reduced to

$$\sin^2 T=\frac{1}{\lambda u_S}\sinh(\pi u_S/2)\cosh(\pi u_S/2)\times[1-\lambda u_S\tanh(\pi u_S/2)], \tag{43}$$

which is the same as the result obtained by Nehring *et al.* [5].

On the other hand, with the condition $\gamma=1$, Eqs. (39) and (40) give

$$\sin^2 T=\cosh^2(\pi Y/2)\left[1-\frac{k_{33}}{k_{11}}\lambda Y\tanh(\pi Y/2)\right], \tag{44}$$

$$\tan\phi_0^S=\tan T\left[1-\frac{k_{11}}{k_{33}\lambda Y}\tanh(\pi Y/2)\right]. \tag{45}$$

This is in agreement with the result reported in Ref. [9].

We have calculated numerically the λ and γ dependencies of the reduced voltage u_S and the surface twist angle ϕ_0^S at the saturation, using the same values of parameters as those in Fig. 4. The result is represented in Fig. 5. It is clear that ϕ_0^S is again strongly dependent on γ, whereas the dependency of u_S on γ is not so notable, except the unrealistic case with $\gamma=\infty$. From Figs. 4(b) and 5(b), it can be concluded that the total twist angle of the liquid-crystal slab, and thus the optical properties of the TN cell, are closely relevant to the azimuthal anchoring.

Figures 4(a) and 5(a) show that for certain values of γ, the $u_F(\lambda)$ and $u_S(\lambda)$ curves intersect. For weaker anchoring conditions with λ larger than its value at the intersection point, the saturation voltage is lower than the threshold voltage, and the liquid-crystal cell is bistable [6]. Detailed analysis reveals that there exists a critical value γ_c for the TN effect with $l/p_0=0$,

$$\gamma_c=\frac{2\sqrt{k_{33}/k_{11}+1}}{\sqrt{3k_{33}^2/k_{22}^2-3}+\sqrt{k_{33}/k_{11}+1}}. \tag{46}$$

When $0\leqslant\gamma\leqslant\gamma_c$, $u_F(\lambda)$ and $u_S(\lambda)$ curves do not intersect, and the liquid-crystal cell is monostable; when $\gamma>\gamma_c$, $u_F(\lambda)$ and $u_S(\lambda)$ curves intersect, and the liquid-crystal cell is monostable or bistable depending on the value of λ. For the typical values of parameters illustrated in Fig. 5(a), we have $\gamma_c\approx 0.57$. Thus for $\gamma=1$ and ∞, the $u_F(\lambda)$ and $u_S(\lambda)$ curves intersect, in accordance with the results obtained in Refs. [6] and [9]. However, for a usual TN cell, γ should be in the order of magnitude of 0.1 or 0.01, which is far smaller than γ_c, thus usual TN cells have no bistable behavior.

IV. HOMEOTROPIC TO TWISTED-PLANAR TRANSITION

It is not surprising that the results on the TNLC slab with homogeneous planar substrates, expressed by Eqs. (29)–(31) and (39)–(41), can be applied to the liquid-crystal cell with homeotropic substrates, since Eq. (10) depicts the two types of anchoring surfaces in a common form. Reference [8] reported the HTP device consisting of a chiral liquid-crystal slab with negative dielectric anisotropy. Its two homeotropic substrates have been rubbed slightly, along different directions with a cross angle ϕ_t, to introduce in-plane anisotropy. When no voltage is applied between the substrates, the liquid crystal aligns in uniform homeotropic conformation, if the chiral modulus of the liquid-crystal material is not so strong [21]. When a voltage is applied across the cell, the electric field couples to the negative dielectric anisotropy of the liquid crystal, and a structural transition is induced at a threshold voltage $\hat{V}_F$, at which the liquid crystal begins to tilt and twist. Further increase of the voltage to $\hat{V}_S$ finally leads to the saturation configuration which is a twisted planar structure. Experimental observation demonstrated the outstanding

optical property of the HTP cell.

Although in the last section we have always focused on the TNLC slab, the results obtained are not limited to that effect. If $W_p>0$ and $W_a>0$ in Eq. (13), and the dielectric anisotropy of the liquid-crystal material is positive ($\epsilon_a>0$), then the liquid-crystal director transforms from twisted planar alignment to homeotropic alignment with the increase of the voltage. This is the conventional TN effect. On the other hand, if $W_p<0$ and $W_a>0$ in Eq. (13), and the dielectric anisotropy of the liquid-crystal material is negative ($\epsilon_a<0$), then as the voltage across the cell increases, the liquid-crystal director transforms from homeotropic alignment to the twisted planar alignment. This is the HTP effect.

Intuitively, the HTP effect is just the reversal of the TN effect. However, this speculation is not evident in the numerical analysis of the HTP transition reported in Ref. [8], where Eq. (4) was employed to depict the boundary coupling. As shown in Fig. 2(d), the polar diagram of Eq. (4) is singular along the normal to the substrate surface. This is especially fatal to the understanding of the HTP transition, since it proceeds from the homeotropic alignment. Therefore, it is beneficial to employ Eq. (12) to characterize the boundary coupling. By doing so, we have found that the analytical results about the TN effect can also be applied to the HTP transition, if only the following replacements are performed,

$$W_p \leftrightarrow -W_1, \quad W_a \leftrightarrow W_{21}=W_2-W_1. \tag{47}$$

It should be emphasized that with these replacements the equations defining the threshold property of the TN effect generate the relations for the saturation property of the HTP transition, while the equations giving the saturation property of the TN effect lead to the description of the threshold property of the HTP transition. This is convincing evidence that they are reverse effects of each other.

To demonstrate the results of this replacement, we define the dimensionless parameters

$$\begin{aligned} \hat{\lambda}&=\pi k_{33}/(2lW_1),\\ \hat{\gamma}&=W_{21}/W_1,\\ \hat{u}_F&=\hat{V}_F/\hat{V}_c,\\ \hat{u}_S&=\hat{V}_S/\hat{V}_c, \end{aligned} \tag{48}$$

where $\hat{V}_c=\pi(k_{33}/|\epsilon_a|)^{1/2}$ is the threshold voltage of a homeotropically aligned slab of an achiral liquid crystal with rigid boundary coupling ($W_{21}=0, W_1\to\infty$). In this section the notations with a caret denote the quantities of the HTP effect.

Using Eqs. (47) and (48), we can determine the threshold property of the HTP transition from modifying Eqs. (39)–(41) (see the Appendix for more details),

$$\sin^2 T=\frac{1}{\hat{\gamma}}\cos^2\left(\frac{\pi\hat{Y}}{2}\right)\left[1+\frac{1+\hat{\gamma}}{\hat{\lambda}\hat{Y}}\tan\left(\frac{\pi\hat{Y}}{2}\right)\right]\times\left[\hat{\lambda}\hat{Y}\tan\left(\frac{\pi\hat{Y}}{2}\right)-1\right], \tag{49}$$

$$\tan\hat{\phi}_0^F=\tan T\left[1+\frac{1}{\hat{\lambda}\hat{Y}}\tan\left(\frac{\pi\hat{Y}}{2}\right)\right]\left[1+\frac{1+\hat{\gamma}}{\hat{\lambda}\hat{Y}}\tan\left(\frac{\pi\hat{Y}}{2}\right)\right]^{-1}, \tag{50}$$

$$\hat{u}_F=\left[\hat{Y}^2-\left(\frac{2lk_{22}}{p_0k_{33}}\right)^2\right]^{1/2}. \tag{51}$$

In these equations, the hyperbolic functions in Eqs. (39)–(41) have changed into trigonometric functions. The minus sign on the right-hand side of Eq. (51) implies that $\hat{u}_F$ can be zero or even imaginary, i.e., the transition may occur spontaneously in zero voltage, if p_0 is short enough. This will be discussed later.

Similarly, the modification of Eqs. (29)–(31) generates the equations of the saturation property of the HTP transition,

$$\phi_t-2\hat{\phi}_0^S-\frac{2\pi l}{p_0}=\frac{\pi\hat{\gamma}k_{33}}{2\hat{\lambda}k_{22}}\sin 2\hat{\phi}_0^S, \tag{52}$$

$$1+\hat{\gamma}\sin^2\hat{\phi}_0^S=\frac{k_{11}}{k_{33}}\hat{\lambda}\hat{X}\tanh\left(\frac{\pi\hat{X}}{2}\right), \tag{53}$$

$$\hat{u}_S=\left(\frac{k_{11}}{k_{33}}\right)^{1/2}\left[\hat{X}^2-\frac{(k_{33}-2k_{22})\Delta\hat{\phi}^2}{k_{11}\pi^2}-\frac{4lk_{22}\Delta\hat{\phi}}{p_0k_{11}\pi}\right]^{1/2}, \tag{54}$$

where $\Delta\hat{\phi}=\phi_t-2\hat{\phi}_0^S$ is the total twist of the liquid crystal at the saturation.

As a special case, taking $p_0=\infty$ and $\hat{\gamma}=0$ in Eqs. (51)–(54), we get

$$\hat{\lambda}\hat{u}_F\tan(\pi\hat{u}_F/2)=1, \tag{55}$$

$$\hat{\lambda}\hat{u}_S\left(\frac{k_{11}}{k_{33}}\right)^{1/2}\tanh\left[\frac{\pi}{2}\left(\frac{k_{33}}{k_{11}}\right)^{1/2}\hat{u}_S\right]=1. \tag{56}$$

This is in good accordance with RP's original result on the homeotropic liquid-crystal cell [4].

The realization of HTP transition relies on the uniform homeotropic alignment of liquid crystal when no voltage is applied. This imposes a restriction on the thickness of the liquid-crystal cell, for the chirality-induced twist is not advantageous to the stability of this initial alignment. Taking $\hat{u}_F=0$ and $\hat{\gamma}=0$ (noting the fact that $W_{21}\ll W_1$ in the experiment [8]), we can derive from Eqs. (51) and (49)

$$\tan\left(\frac{\pi Lk_{22}}{p_0k_{33}}\right)=\frac{p_0}{\pi k_{22}}W_1, \tag{57}$$

where L is the critical thickness of the cell: if $l<L$, the uniform homeotropic alignment is stable. In the rigid anchoring limit, $W_1\to\infty$, L reaches its maximal value

$$\frac{L}{p_0}=\frac{k_{33}}{2k_{22}}. \tag{58}$$

Noting the fact that usually $k_{33}\sim 2k_{22}$, this relation implies that the critical cell thickness is approximate to the pitch of the liquid crystal, $L\sim p_0$. This is in good agreement with the result about the rigid-anchoring homeotropic cell reported previously [21]. Equation (57) also indicates that L decreases for weaker boundary coupling W_1. Nevertheless, $l=p_0/4$ is safe for the building of the homeotropic alignment, as has been done in Ref. [8].

The present result on the HTP effect expressed by Eqs. (51)–(54) is not consistent with the numerical result reported in Ref. [8]. For example, as reported there, the azimuthal angle $\hat{\phi}_0$ is always approximate to zero, and the total twist angle $\phi_t-2\hat{\phi}_0^F$ is a constant ϕ_t ($=\pi/2$ there). For comparison, noting that $W_{21}\ll W_1$ or $\hat{\gamma}\ll 1$ in the experiment, we can derive from Eq. (50) that, at least at the threshold,

$$\hat{\phi}_0^F\simeq T=\frac{\phi_t}{2}-\frac{\pi l k_{22}}{p_0 k_{33}}. \tag{59}$$

Taking $\phi_t=\pi/2$, $l=p_0/4$, and $k_{22}/k_{33}=0.5$, we have $\hat{\phi}_0^F\simeq\pi/8$, and the total twist angle $\phi_t-2\hat{\phi}_0^F\simeq\pi/4$ is just half of the value reported in Ref. [8]. This notable difference should be meaningful to the understanding of the optical properties of the HTP cell. In its origin, $\hat{\phi}_0\equiv 0$ reported in Ref. [8] is a consequence of the expression of the anchoring energy Eq. (4). As shown in Fig. 2(d), there is a finite difference of the anchoring energy between the $(\theta_0=0,\phi_0=0)$ and $(\theta_0=0,\phi_0=\pi/2)$ directions, though they are physically identical. This determines that $\hat{\phi}_0$ must be zero at least near the threshold, for the bulk elastic energy of infinitesimal distortion must be dominated by the finite difference of the surface energy. This indicates that the singular expression Eq. (4) cannot lead to proper understanding of the HTP transition.

In Fig. 6, we plot the anchoring dependencies of the threshold and saturation properties of the HTP effect calculated based on Eqs. (51)–(54). The material parameters used are $k_{11}/k_{33}=1$ and $k_{22}/k_{33}=0.5$. The ratio $l/p_0=0.25$ is to follow the initial idea in Ref. [8]. The threshold and saturation voltages of the HTP cell are hardly dependent on $\hat{\gamma}$ or the azimuthal anchoring, whereas the surface twist angle $\hat{\phi}_0^F$ at the threshold is affected by the azimuthal anchoring in a much greater extent. For small γ (<0.1), $\hat{\phi}_0^F$ is approximate to $\pi/8$, in agreement with the evaluation performed above. Due to the values of parameters, the surface twist angle $\hat{\phi}_0^S$ at the saturation is always zero, independent of both $\hat{\lambda}$ and $\hat{\gamma}$; the saturation voltage $\hat{u}_S$ is independent from $\hat{\gamma}$.

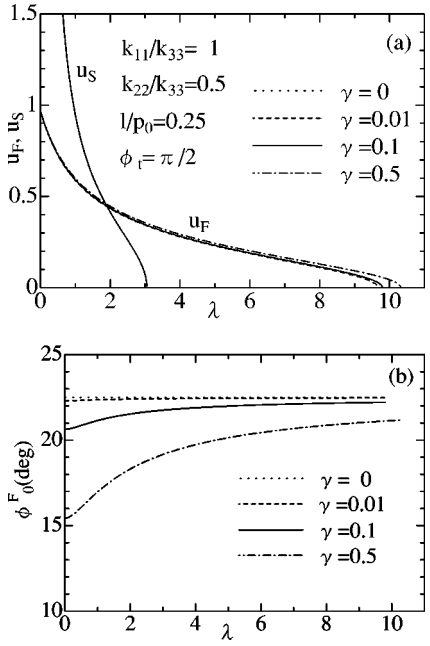

FIG. 6. $\hat{\lambda}$ and $\hat{\gamma}$ dependencies of the threshold and saturation properties of the homeotropic to twisted-planar transition. (a) The reduced threshold ($\hat{u}_F$) and saturation ($\hat{u}_S$) voltages; (b) the surface twist angle $\hat{\phi}_0^F$ at threshold. The parameters used are $k_{11}/k_{33}=1$, $k_{22}/k_{33}=0.5$, $l/p_0=0.25$, and $\phi_t=\pi/2$. Owing to the values of these parameters, the surface twist angle $\hat{\phi}_0^S$ at saturation is always zero and not plotted; the saturation voltage $\hat{u}_S$ is independent from $\hat{\gamma}$.

V. CONCLUSIONS

In this paper, we have studied the surface anchoring of liquid crystals. Through spherical harmonic expansion of the surface energy, a two-term expression of the anchoring energy is derived, which is highly symmetric, as is embodied by the anchoring triplet $(\vec{\xi},\vec{\eta},\vec{\epsilon})$, and shown in Figs. 2(e) and 2(f).

Using the present expression of the anchoring energy, we have made a rigorous analysis of weak boundary coupling effects for structural transitions of nematic liquid crystals. The threshold and saturation properties of TN effect are derived in detail. The formulas obtained for TN effect have been applied to the HTP transition based on the fact that the present anchoring energy depicts the homogeneous planar and the homeotropic anchoring surfaces uniformly. Our analysis shows that the TN and the HTP transitions are actually reverse effects of each other. These results improve our understanding of these structural transitions.

APPENDIX

1. Derivation of Eqs. (29)–(31)

For convenience, we introduce a variable α,

$$\cos\theta=\cos\theta_M\sin\alpha,\quad(\cos\theta_0=\cos\theta_M\sin\alpha_0). \tag{A1}$$

Substituting this equation into Eqs. (24)–(26), then taking the limit $\theta_M\to\pi/2$, we get, respectively,

$$\frac{\pi X}{2}=\frac{\pi}{2}-\alpha_0, \tag{A2}$$

$$\frac{\phi_t}{2}-\phi_0^F=\left(\frac{\pi}{2}-\alpha_0\right)\left(\frac{C_1-k_2}{k_{22}}\right)\frac{l}{\pi X}, \tag{A3}$$

$$W_p-W_a\sin^2\phi_0^F=\frac{\pi k_{11}X}{2l}\cot\alpha_0, \tag{A4}$$

where $C_1=W_a\sin 2\phi_0^F$, as reduced from Eq. (23), and

$$X=\left\{\frac{\epsilon_a V_F^2}{\pi^2 k_{11}}+\frac{l^2}{\pi^2 k_{11}k_{22}^2}[(2k_{22}-k_{33})(C_1-k_2)^2 + 2k_2k_{22}(C_1-k_2)]\right\}^{1/2}. \tag{A5}$$

The threshold voltage V_F and the surface twist angle ϕ_0^F should be determined by Eqs. (A2)–(A5).

Using the parameters defined by Eq. (28), the ratio of Eq. (A3) to Eq. (A2) gives Eq. (29), the elimination of α_0 from Eqs. (A2) and (A4) gives Eq. (30), and Eq. (A5) reduces to Eq. (31).

2. Derivation of Eqs. (39)–(40)

Introduce a variable β,

$$\sin\theta=\frac{\sin\theta_M}{\cos\beta},\quad \left(\sin\theta_0=\frac{\sin\theta_M}{\cos\beta_0}\right). \tag{A6}$$

Substituting this equation into Eqs. (24)–(26), then taking the limit $\theta_M\to 0$, we get

$$\frac{\sin\beta_0}{\sqrt{Y^2+q^2\cos^2\beta_0}}=\frac{1}{Y}\tanh\left(\frac{\pi Y}{2}\right), \tag{A7}$$

$$T-\phi_0^S=\sin^{-1}\left(\frac{q\sin\beta_0}{\sqrt{Y^2+q^2}}\right), \tag{A8}$$

$$W_p-W_a\sin^2\phi_0^S=\frac{\pi k_{33}}{2l}\sin\beta_0\sqrt{Y^2+q^2\cos^2\beta_0}, \tag{A9}$$

respectively, where

$$q=\frac{lW_a\sin 2\phi_0^S}{\pi k_{33}\cos^2\beta_0}. \tag{A10}$$

The relation between Y and the reduced saturation voltage $u_S=V_S/V_c$ is expressed by Eq. (41).

Eliminating β_0 from Eqs. (A7) and (A9), we can express ϕ_0^S via Y as

$$\sin^2\phi_0^S=\frac{1+\eta^2\lambda^2Y^2-\eta\lambda Y[\tanh(\pi Y/2)+\coth(\pi Y/2)]}{\gamma\{(2-\gamma)-\eta\lambda Y[\tanh(\pi Y/2)+\coth(\pi Y/2)]\}}, \tag{A11}$$

where $\eta=k_{33}/k_{11}$, and the dimensionless parameters defined in Eq. (28) are used.

Using Eq. (A11) to simplify Eq. (A8), after a lengthy calculation, we can eliminate β_0 and ϕ_0^S, and obtain Eq. (39). Finally, using Eq. (39) we can rewrite Eq. (A11) to Eq. (40).

3. Derivation of Eqs. (51)–(54)

From Eqs. (47) and (48), we can get the following replacement relations:

$$\gamma\leftrightarrow-\hat{\gamma},\quad \lambda\leftrightarrow-\frac{k_{11}}{k_{33}}\hat{\lambda}. \tag{A12}$$

Since in the TN effect and the HTP effect, the twisted planar, twisted tilt, and homeotropic configurations appear in reverse order, it is natural that the threshold and the saturation voltages of the two effects are exchanged,

$$u_F\leftrightarrow i\left(\frac{k_{33}}{k_{11}}\right)^{1/2}\hat{u}_S,\quad u_S\leftrightarrow i\left(\frac{k_{33}}{k_{11}}\right)^{1/2}\hat{u}_F, \tag{A13}$$

where the imaginary unit i comes from the opposite signs of ϵ_a in the definitions of V_c and $\hat{V}_c$. The variables X and Y employed in Sec. III have to be treated carefully. It should be noted that there is a factor λ or γ^{-1} on the right-hand side of Eqs. (30) and (39). Due to the negative signs in Eq. (A12), X and Y determined by these relations should become imaginary. For convenience, we introduce variables $\hat{X}$ and $\hat{Y}$, and request them to satisfy the following replacement relations:

$$X\leftrightarrow i\hat{X},\quad Y\leftrightarrow i\hat{Y}. \tag{A14}$$

The substitution of Eqs. (A12)–(A14) into Eqs. (39)–(41) generates Eqs. (49)–(51). The same substitution into Eqs. (29)–(31) generates Eqs. (52)–(54).

[1] A. A. Sonin, *The Surface Physics of Liquid Crystals* (Gordon and Breach, London, 1995).
[2] J. Cognard, Mol. Cryst. Liq. Cryst. Suppl. Ser. **1**, 1 (1982).
[3] B. Jérôme, Rep. Prog. Phys. **54**, 391 (1991).
[4] A. Rapini and M. Papoular, J. Phys. (Paris), Colloq. **30**, C4.54 (1969).
[5] J. Nehring, A. R. Kmetz, and T. J. Scheffer, J. Appl. Phys. **47**, 850 (1976).
[6] M. E. Becker, J. Nehring, and T. J. Scheffer, J. Appl. Phys. **57**, 4539 (1985).
[7] R. Hirning, W. Funk, J.-R. Trebin, M. Schmidt, and H. Schmiedel, J. Appl. Phys. **70**, 4211 (1991).

[8] S.-W. Suh, S. T. Shin, and S.-D. Lee, Appl. Phys. Lett. **68**, 2819 (1996); Mol. Cryst. Liq. Cryst. Sci. Technol., Sect. A **302**, 163 (1997).

[9] A. Sugimura and Z. Ou-Yang, Phys. Rev. E **51**, 784 (1995); A. Sugimura, G. R. Luckhurst, and Z. Ou-Yang, *ibid.* **52**, 681 (1995).

[10] T. Beica, S. Frunza, R. Moldovan, and D. N. Stoenescu, Mol. Cryst. Liq. Cryst. Sci. Technol., Sect. A **301**, 39 (1997).

[11] Assuming $g_s(\theta_0,\phi_0)=g_s^z(\theta_0)+g_s^a(\phi_0)$, let us pay attention to the surface normal $\theta_0=0$. We have $g_s|_{\theta_0=0}=\text{Const.}+g_s^a(\phi_0)$. This means that an infinitude of values of g_s exist in the normal direction corresponding to the infinitude of values of ϕ_0. This unphysical dependence upon ϕ_0 leads to the singularity along the surface normal, as illustrated in Figs. 2(b), 2(c), and 2(d).

[12] C. V. Brown, M. J. Towler, V. C. Hui, and G. P. Bryan-Brown, Liq. Cryst. **27**, 233 (2000).

[13] W. Zhao, C.-X. Wu, and M. Iwamoto, Phys. Rev. E **62**, R1481 (2000).

[14] G. P. Bryan-Brown, C. V. Brown, I. C. Sage, and V. C. Hui, Nature (London) **392**, 365 (1998).

[15] P. Pieranski and B. Jérôme, Phys. Rev. A **40**, 317 (1989).

[16] P. G. de Gennes and J. Prost, *The Physics of Liquid Crystals*, 2nd ed. (Clarendon, Oxford, 1993).

[17] K. H. Yang, Appl. Phys. Lett. **43**, 171 (1983).

[18] M. Jiang, X. Huang, Z. Wang, K. Ma, Q. Sun, and X. Zhang, Liq. Cryst. **18**, 419 (1995).

[19] F. M. Leslie, Mol. Cryst. Liq. Cryst. **12**, 57 (1970).

[20] M. Schadt and W. Helfrich, Appl. Phys. Lett. **18**, 127 (1971).

[21] P. Ribiere, S. Pirkl, and P. Oswald, Phys. Rev. A **44**, 8198 (1991).